

A GENERAL HIGH-ORDER MULTI-DOMAIN HYBRID DG/WENO-FD METHOD FOR HYPERBOLIC CONSERVATION LAWS*

Jian Cheng, Kun Wang and Tiegang Liu

School of Mathematics and Systems Science, Beihang University, Beijing, China

Email: chengjian@buaa.edu.cn, wangkun@buaa.edu.cn, liutg@buaa.edu.cn

Abstract

In this paper, a general high-order multi-domain hybrid DG/WENO-FD method, which couples a p^{th} -order ($p \geq 3$) DG method and a q^{th} -order ($q \geq 3$) WENO-FD scheme, is developed. There are two possible coupling approaches at the domain interface, one is non-conservative, the other is conservative. The non-conservative coupling approach can preserve optimal order of accuracy and the local conservative error is proved to be upmost third order. As for the conservative coupling approach, accuracy analysis shows the forced conservation strategy at the coupling interface deteriorates the accuracy locally to first-order accuracy at the ‘coupling cell’. A numerical experiments of numerical stability is also presented for the non-conservative and conservative coupling approaches. Several numerical results are presented to verify the theoretical analysis results and demonstrate the performance of the hybrid DG/WENO-FD solver.

Mathematics subject classification: 65M60, 65M99, 35L65

Key words: Discontinuous Galerkin method, Weighted essentially nonoscillatory scheme, Hybrid methods, high-order scheme.

1. Introduction

In recent years, high-order methods with low numerical diffusion and dispersion errors have been extensively studied and widely used for resolving complex fluid structures and capturing vortex evolution. Many kinds of high-order methods have been developed over the past two decades, especially high-order finite difference (FD) type methods, such as weighted essentially non-oscillatory (WENO) schemes [10,11], high-order finite volume (FV) type methods [12,29,30] and discontinuous Galerkin (DG) type methods, which includes traditional Runge-Kutta discontinuous Galerkin (RKDG) methods [1,2], spectral volume (SV) methods [19,20], spectral difference (SD) method [14], correction procedure via reconstruction (CPR) schemes [13,21] and so on. FD type methods are generally considered as highly efficient and easily achieve high-order accuracy on structured grids. FV type methods, compared to the FD type methods, have flexibility in handling almost arbitrary grid with reasonable computational cost, however, they usually are not compact when extends to high order accuracy. DG type methods can treat complex geometries through a compact stencil as each cell only communicates with its immediate face-neighbors through approximate Riemann solvers. However, they are generally more time consuming than the FV type methods.

As all of those high-order methods mentioned above have their advantages and disadvantages, several hybrid methods have been developed in order to locally take the advantages of

* Received April 18, 2014 / Revised version received June 22, 2015 / Accepted October 16, 2015 /
Published online January 18, 2016 /

different types of methods above. There are mainly two kinds of hybrid approaches in literature, one is based on local polynomial reconstruction, the other is based on computational domain decomposition.

Based on local polynomial reconstruction, one of the most typical and successful implementation is WENO/Hermite WENO type limiter for DG methods [4-7]. The basic idea of WENO/Hermite WENO limiter is to use the local polynomial reconstruction of WENO type to replace the original reconstruction approach of DG methods for high-order degrees of freedom at the ‘troubled cells’. Such hybrid approach preserves essentially non-oscillatory property for those cells near the area of discontinuities. In fact, the strategy can be applied for all the cells rather than only for those ‘troubled cells’. Luo et al. [3, 8, 9] adopted this strategy and developed a kind of reconstructed DG methods (rDG) which reconstructs high-order degrees of freedom using a least-squares technique in 2D and a hierarchical WENO reconstruction in 3D. This hybrid approach combines the efficiency of reconstruction methods widely used in FV type schemes and the accuracy and robustness of DG methods. Similarly, based on local polynomial reconstruction, Dumbser et al. [15] presented a unified framework for constructing one step finite volume and discontinuous Galerkin schemes on unstructured meshes, resulting in a class of PnPm schemes. Zhang et al. [16–18] introduced a hybrid DG/FV method. In their hybrid DG/FV method, a DG method based on Taylor basis functions was adopted to compute the low-order degrees of freedom. A high order finite volume method is then used to reconstruct high-order derivatives with the known low-order derivatives.

Based on computational domain decomposition, a multi-domain hybrid spectral-WENO method was introduced by Costa et al. [22] for hyperbolic conservation laws. The hybrid spectral-WENO method conjugates the non-oscillatory properties of high-order WENO schemes and the high efficiency and accuracy of spectral methods in a multi-domain approach. Recently, Shahbazi et al. [23] introduced a multi-domain Fourier-continuation/WENO hybrid solver for conservation laws. In the area of CAA, Utmann et al. [26, 28] and Léger et al. [27] developed a coupled DG/FD method for computational aeroacoustics. The coupled DG/FD solver approximates the solution in the close neighborhood of complex obstacles with an unstructured grids and computes the rest of the field on structured grids in order to alleviate computational cost.

In our previous work [31, 32], we introduced a class of multi-domain hybrid DG and WENO-FD method based on a third-order DG method and a fifth-order WENO-FD scheme for the purpose of saving computational cost and treating complex geometry. We found that the conservative coupling approach deteriorates the accuracy seriously and only the non-conservative coupling approach can preserve third-order accuracy. Thus, a special treatment was developed in our previous work: the non-conservative coupling approach is employed when the solution is smooth enough and it is replaced by the conservative coupling approach when there are possible discontinuities passing through the interface.

In this paper, as a direct extension of our previous work, two main issues will be addressed: one is whether the hybrid method can be extended to arbitrary high-order accuracy, the other is whether the hybrid method can preserve numerical stability with different choices of numerical fluxes at coupling interface. Firstly, we extend the previous third-order hybrid DG/WENO-FD method to a more general situation which couples a p^{th} -order ($p \geq 3$) DG method with a q^{th} -order ($q \geq 3$) WENO-FD scheme. We present a general analysis of accuracy and conservative error for this general high-order hybrid DG/WENO-FD method. From the theoretical analysis, as we will see later, the conservative coupling approach of a p^{th} -order DG method and a q^{th} -order WENO-FD scheme is only of first-order accuracy locally at the ‘coupling cell’ and the

accuracy order is independent from the choices of numerical fluxes at the coupling interface. In contrast, the non-conservative coupling approach can preserve optimal r^{th} -order ($r = \min(p, q)$) accuracy in the whole computational domain while at the same time the local conservative error is proved to be upmost third order. Secondly, numerical analysis and comparison of stability for the non-conservative and conservative coupling approaches is presented. Numerical experiments demonstrate that the non-conservative coupling approach can preserve numerical stability. For the conservative coupling approach, it can be seen that in some situation the conservative coupling approach with WENO-FD flux employed at the coupling interface can lead to linear instability. However, when the nonlinear factors are taken into consideration, both using DG flux and using WENO-FD flux can preserve numerical stability.

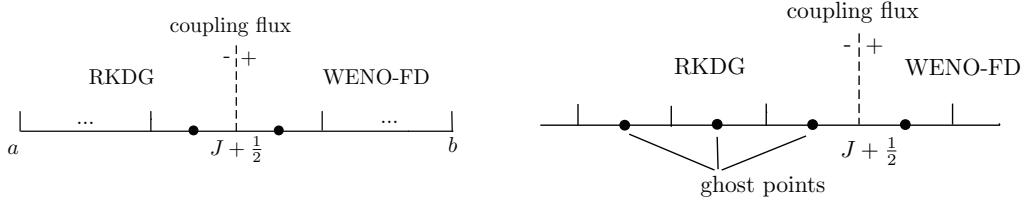
The rest of this paper is arranged as follows. In Section 2, we give a detail description of the general high-order hybrid DG/WENO-FD method. In Section 3, we present the general analysis results of accuracy, stability and conservative error for the conservative and non-conservative coupling approaches, respectively. In Section 4, numerical experiments of a hybrid 3^{rd} -order DG/ 5^{th} -order WENO-FD method together with a hybrid 5^{th} -order DG/ 5^{th} -order WENO-FD method are used to verify our theoretical results and demonstrate the performance of the high-order hybrid solver. Finally, Section 5 contains concluding remarks.

2. A General High-order Hybrid DG/WENO-FD Method

In this section, we give a detail description of the high-order hybrid DG/WENO-FD method, we will focus on the implementation for the scalar conservation law:

$$u_t + \sum_{i=1}^d (f_i(u))_{x_i} = 0, \quad (2.1)$$

where $u = (u_1, \dots, u_m)^t$, $x = (x_1, \dots, x_d)$. For simplicity, we use the special case of (2.1) with $d = m = 1$ as a model to illustrate the method. Assume that the computational domain



(a) Domain decomposition in one dimension.

(b) Ghost nodes for constructing the WENO-FD flux of a 5^{th} -WENO-FD scheme.

Fig. 2.1. Multi-domain hybrid methods for one dimensional problems.

$$a = x_{\frac{1}{2}} < x_{\frac{3}{2}} < \dots < x_{N+\frac{1}{2}} = b,$$

as shown in Fig. 2.1(a), is divided into two subdomains with the multi-domain interface located at $x = x_{J+1/2}$.

In the left subdomain $(x_{1/2}, x_{J+1/2})$, a traditional high-order DG method is applied as follows

$$\frac{du_j^{(l)}}{dt} + \frac{1}{w_l} \left[\Delta_- \left(v_l^j(x_{j+\frac{1}{2}}) \tilde{f}_{j+\frac{1}{2}}^{(rkdg)} \right) \right] - \frac{1}{w_l} \int_{I_j} f(u^h(x, t)) \frac{d}{dx} v_l^j(x) dx = 0, \quad l = 0, 1, 2, \dots, k, \quad (2.2)$$

where $\widehat{f}_{j+\frac{1}{2}}^{(rkdg)}$ is the DG flux at cell interface $I_{j+\frac{1}{2}}$ and

$$\Delta_- \omega_j = \omega_j - \omega_{j-1}, \Delta_+ \omega_j = \omega_{j+1} - \omega_j.$$

In this work, a set of local orthogonal Legendre polynomial basis $v_l^j(x), l = 0, 1, 2, \dots, k$ is adopted with the definition of $w_l = \int_{I_j} (v_l^j(x))^2 dx$. In the right subdomain $(x_{J+1/2}, x_{N+1/2})$, a high-order WENO-FD scheme is adopted in this work

$$\frac{d}{dt} u_j + \frac{1}{\Delta x_j} \left(\widehat{f}_{j+\frac{1}{2}}^{(weno)} - \widehat{f}_{j-\frac{1}{2}}^{(weno)} \right) = 0, \quad (2.3)$$

where $\widehat{f}_{j+\frac{1}{2}}^{(weno)}$ is the WENO-FD flux at cell interface and Δx_j is the mesh size of cell I_j .

Then, the general semi-discrete form of the multi-domain hybrid DG/WENO-FD method defined on (a, b) can be expressed as follows:

$$\begin{cases} \frac{d}{dt} u_j + \frac{1}{\Delta x_j} \left(\widehat{f}_{j+\frac{1}{2}}^{(rkdg)} - \widehat{f}_{j-\frac{1}{2}}^{(rkdg)} \right) = 0, & j = 1, \dots, J-1, \\ \frac{d}{dt} u_j + \frac{1}{\Delta x_j} \left(\widehat{f}_{j+\frac{1}{2}}^{(I^-)} - \widehat{f}_{j-\frac{1}{2}}^{(rkdg)} \right) = 0, & j = J, \\ \frac{d}{dt} u_j + \frac{1}{\Delta x_j} \left(\widehat{f}_{j+\frac{1}{2}}^{(weno)} - \widehat{f}_{j-\frac{1}{2}}^{(I^+)} \right) = 0, & j = J+1, \\ \frac{d}{dt} u_j + \frac{1}{\Delta x_j} \left(\widehat{f}_{j+\frac{1}{2}}^{(weno)} - \widehat{f}_{j-\frac{1}{2}}^{(weno)} \right) = 0, & j = J+2, \dots, N. \end{cases} \quad (2.4)$$

where u_j represents point values for the WENO-FD subdomain and cell averaged values (zero degree of freedom) for the DG subdomain. At the coupling interface, the numerical flux employed in the DG subdomain is denoted by $\widehat{f}_{j+\frac{1}{2}}^{(I^-)}$ and the numerical flux employed in the WENO-FD subdomain is denoted by $\widehat{f}_{j+\frac{1}{2}}^{(I^+)}$.

It should be noted that at the multi-domain coupling interface $x = x_{J+1/2}$, there are two numerical fluxes $\widehat{f}_{J+\frac{1}{2}}^{(I^-)}$ and $\widehat{f}_{J+\frac{1}{2}}^{(I^+)}$. If we have

$$\widehat{f}_{J+\frac{1}{2}}^{(I^-)} = \widehat{f}_{J+\frac{1}{2}}^{(I^+)}, \quad (2.5)$$

then we call it the conservative coupling approach. Otherwise, if

$$\widehat{f}_{J+\frac{1}{2}}^{(I^-)} \neq \widehat{f}_{J+\frac{1}{2}}^{(I^+)}, \quad (2.6)$$

which means different numerical fluxes are applied for different subdomains at the same coupling interface, thus we call this coupling approach non-conservative.

2.1. Construct numerical fluxes at coupling interface

In this subsection, we present the strategies of constructing numerical fluxes $\widehat{f}_{J+1/2}^{(weno)}$ and $\widehat{f}_{J+1/2}^{(rkdg)}$ for the WENO-FD subdomain and DG subdomain, respectively, at the coupling interface $x = x_{J+1/2}$.

Similar to the strategy used in [33] for multi-domain WENO-FD method, it is easy in the construction of numerical flux $\widehat{f}_{J+1/2}^{(weno)}$ for the WENO-FD subdomain as the DG subdomain can provide the approximate point values for the WENO-FD scheme. In detail, in order to construct the numerical flux $\widehat{f}_{J+1/2}^{(weno)}$ of a q^{th} -order ($q = 2r - 1$) WENO-FD scheme, we need r WENO-FD point values

$$u_{J-r+1}^{(weno)}, u_{J-r+2}^{(weno)}, \dots, u_J^{(weno)}$$

at $x_{J-r+1}, x_{J-r+2}, \dots, x_J$, which are located in the DG subdomain and called ghost points. For example, we show these ghost points used for constructing the numerical flux for a 5th-order WENO-FD scheme in Fig. 2.1(b). These point values are simply calculated from the approximate solution polynomial of a p^{th} -order DG method:

$$u^h(x, t) = \sum_{l=0}^{p-1} u_j^{(l)}(t) \varphi_l^{(j)}(x), \quad x \in I_j, \quad (2.7)$$

where $u_j^{(l)}(t)$ are degrees of freedom in the cell I_j and $\varphi_l^{(j)}(x), l = 0, 1, \dots, p-1$ are a set of local orthogonal basis over I_j .

As for the constructing of the numerical flux $\hat{f}_{J+1/2}^{(rkdg)}$ for the DG subdomain, we need get $u_{J+1/2}^+$ and $u_{J+1/2}^-$ at the coupling interface $x_{J+1/2}$ to form the numerical flux. It is obvious that $u_{J+1/2}^-$ at the right boundary of the cell I_J can be obtained by expression (2.7), whereas, $u_{J+1/2}^+$ needs to be reconstructed through the point values from the WENO-FD subdomain. In order to preserve high order accuracy and prevent possible numerical oscillation, a WENO type interpolation is applied to the construction of $u_{J+1/2}^+$. In this procedure, we need a stencil of $2p-1$ points to obtain the Gauss quadrature point values and reconstruct the degrees of freedom for a p^{th} -order DG method in the target cell I_{J+1} . To do so, the following steps are used:

Step 1: Choose $2p-1$ points interpolation stencil $S = \{I_{J-p+2}, \dots, I_{J+p-1}, I_{J+p}\}$ and divide stencil S into p small stencils denoted by

$$S_i = \{I_{J-p+2+i}, \dots, I_{J+i}, I_{J+1+i}\}, \quad i = 0, 1, \dots, p-1;$$

Step 2: Construct an interpolation polynomial $p_i(x)$ associated with each of the stencils $S_i, i = 0, 1, \dots, p-1$ which satisfied $p_i(x_k) = u(x_k), k \in S_i$ and get these approximate point values at each Gauss quadrature point x_G in the cell I_{J+1} of each $p_i(x), i = 0, 1, \dots, p-1$;

Step 3: Obtain the linear weights λ_i , smoothness indicators β_i and calculate the nonlinear weights ω_i of each small stencil $S_i, i = 0, 1, \dots, p-1$ following WENO reconstruction procedures, the final approximate for each Gauss quadrature point x_G is then given by

$$u(x_G) \approx \sum_{i=0}^{p-1} \omega_i p_i(x_G), \quad x_G \in I_{J+1}; \quad (2.8)$$

Step 4: Reconstruct the degrees of freedom for the DG method in the cell I_{J+1} through a numerical integration

$$u_{J+1}^{(l)} = \frac{1}{a_l} \sum_G w_G u(x_G) \varphi_l^{(J+1)}(x_G), \quad l = 0, 1, \dots, p-1, \quad (2.9)$$

where $a_l = \sum_G w_G (\varphi_l^{(J+1)}(x_G))^2$. Then, get the $u_{J+1/2}^+$ through the expression (2.7).

Since we have reconstructed the $u_{J+1/2}^+$ at the right side of the coupling interface $x = x_{J+1/2}$, we can form the DG numerical flux $\hat{f}_{J+1/2}^{(rkdg)}$ for the DG subdomain. The advantages of using WENO interpolation in constructing DG flux is that WENO interpolation can provide $u_{J+1/2}^+$ with the property of essentially non-oscillation. It should be noted that this is crucial in preserving the numerical stability when the DG flux is employed at the coupling interface. Alternatively, we can get $u_{J+1/2}^+$ directly through a WENO interpolation at the coupling interface

$x = x_{J+1/2}$ instead of reconstruction the approximated solution polynomial in the cell I_{J+1} . Numerical experiments demonstrate that actually there is not much difference in obtaining $u_{J+1/2}^+$ directly from this WENO interpolation, thus we also use this simple strategy in some of our numerical experiments.

2.2. Non-conservative and conservative coupling

As the numerical fluxes at the coupling interface are not unique, we have two kinds of coupling approaches at the coupling interface, one is non-conservative, the other is conservative. For the non-conservative approach, we use different numerical fluxes for different subdomains at the same coupling interface $x = x_{J+1/2}$. More specifically, we use

$$\widehat{f}_{J+\frac{1}{2}}^{(I^-)} = \widehat{f}_{J+\frac{1}{2}}^{(rkdg)}, \quad \widehat{f}_{J+\frac{1}{2}}^{(I^+)} = \widehat{f}_{J+\frac{1}{2}}^{(weno)}, \quad (2.10)$$

for the non-conservative coupling approach and the semi-discrete form Eq. (2.4) becomes

$$\begin{cases} \frac{d}{dt} u_j + \frac{1}{\Delta x_j} \left(\widehat{f}_{j+\frac{1}{2}}^{(rkdg)} - \widehat{f}_{j-\frac{1}{2}}^{(rkdg)} \right) = 0, & j = 1, \dots, J, \\ \frac{d}{dt} u_j + \frac{1}{\Delta x_j} \left(\widehat{f}_{j+\frac{1}{2}}^{(weno)} - \widehat{f}_{j-\frac{1}{2}}^{(weno)} \right) = 0, & j = J+1, \dots, N. \end{cases} \quad (2.11)$$

Non-conservative coupling approach demonstrates good performance when the solution is smooth nearby the coupling interface, however, if there is a discontinuity, such as a shock wave, like most of the other non-conservative methods, this coupling approach might suffer from a severe problem in capturing discontinuities correctly. At this moment, conservative coupling approach must be employed at the coupling interface. For this conservative coupling, we can use either the WENO-FD flux or the DG flux as the unique flux at the coupling interface and the semi-discrete form Eq. (2.4) of the conservative coupling approach now becomes

$$\begin{cases} \frac{d}{dt} u_j + \frac{1}{\Delta x_j} \left(\widehat{f}_{j+\frac{1}{2}}^{(rkdg)} - \widehat{f}_{j-\frac{1}{2}}^{(rkdg)} \right) = 0, & j = 1, \dots, J-1, \\ \frac{d}{dt} u_j + \frac{1}{\Delta x_j} \left(\widehat{f}_{j+\frac{1}{2}}^{(I)} - \widehat{f}_{j-\frac{1}{2}}^{(rkdg)} \right) = 0, & j = J, \\ \frac{d}{dt} u_j + \frac{1}{\Delta x_j} \left(\widehat{f}_{j+\frac{1}{2}}^{(weno)} - \widehat{f}_{j-\frac{1}{2}}^{(I)} \right) = 0, & j = J+1, \\ \frac{d}{dt} u_j + \frac{1}{\Delta x_j} \left(\widehat{f}_{j+\frac{1}{2}}^{(weno)} - \widehat{f}_{j-\frac{1}{2}}^{(weno)} \right) = 0, & j = J+2, \dots, N. \end{cases} \quad (2.12)$$

where $\widehat{f}_{J+\frac{1}{2}}^{(I)} = \widehat{f}_{J+\frac{1}{2}}^{(rkdg)}$ or $\widehat{f}_{J+\frac{1}{2}}^{(I)} = \widehat{f}_{J+\frac{1}{2}}^{(weno)}$.

2.3. Hybrid DG/WENO-FD method

The theoretical analysis in the next section will show that there are both advantages and disadvantages for non-conservative and conservative approaches. In practical application, we firstly detect possible discontinuities near the coupling interface, then choose the appropriate coupling approach in the hybrid DG/WENO-FD method.

In order to detect those possible discontinuities near the coupling interface $x = x_{J+1/2}$, a feasible way is to use the so-called ‘troubled cell’ indicator [4, 5]. We call a cell ‘troubled cell’ if the cell is indicated to possibly include a discontinuity. Thus, if either of the neighbor cells near the coupling interface is identified as a ‘troubled cell’, it is wise to use the conservative coupling approach rather than the non-conservative one. That means the hybrid method comes back to be conservative when a discontinuity is passing through the coupling interface. In practice, we

follow our previous work [31, 32] and use a TVD(TVB) minmod function as the ‘troubled cell’ indicator as follow

$$\tilde{u}_k^{(mod)} = m(\tilde{u}_k, \Delta_+ u_k, \Delta_- u_k), \quad \tilde{\tilde{u}}_k^{(mod)} = m(\tilde{\tilde{u}}_k, \Delta_+ u_k, \Delta_- u_k), \quad k = J, J+1 \quad (2.13)$$

where $\tilde{u}_k = u_{k+\frac{1}{2}}^- - \bar{u}_k$, $\tilde{\tilde{u}}_k = \bar{u}_k - u_{k-\frac{1}{2}}^+$, $\Delta_+ u_k = \bar{u}_{k+1} - \bar{u}_k$, $\Delta_- u_k = \bar{u}_k - \bar{u}_{k-1}$ and $m(a_1, a_2, a_3)$ is the TVD (TVB) minmod function. It should be noted that for the RKDG subdomain, the zero degree of freedom $u_k^{(0)}$ is used as the cell average \bar{u}_k and for the WENO-FD subdomain, the cell average \bar{u}_k is provided by the high order integration polynomial $p(x)$ described in Section 2.1.

Finally, we summary the procedure of the multi-domain hybrid DG/WENO-FD method in following steps:

Step 1: Initialize degrees of freedom for the DG subdomain and point values for the WENO-FD subdomain;

Step 2: Construct numerical fluxes $\hat{f}_{J+1/2}^{(weno)}$ and $\hat{f}_{J+1/2}^{(rkdg)}$ at the coupling interface, respectively;

Step 3: Detect the possible discontinuities in the neighbor cells I_J and I_{J+1} of the coupling interface: If neither of these two neighbor cells is identified as a ‘troubled cell’, the non-conservative coupling approach is adopted; Otherwise, the conservative coupling approach is applied with an unique numerical flux $\hat{f}_{I+1/2, J}^{(weno)}$ or $\hat{f}_{I+1/2, J}^{(rkdg)}$ used at the coupling interface;

Step 4: Complete the space discretization for the DG subdomain and the WENO-FD subdomain.

As for the time discretization, an explicit third-order TVD Runge-Kutta method is used with a CFL number equal to the minimum of the CFL numbers of all the subdomains. It should be noticed that the strategy of choosing CFL is straight forward, however, may be not optimal, as for real application, a local time stepping procedure should be more appropriate.

Finally, the third-order TVD Runge-Kutta method is given as follows

$$u^{(1)} = u^n + \Delta t L(u^n), \quad (2.14a)$$

$$u^{(2)} = \frac{3}{4}u^n + \frac{1}{4}u^{(1)} + \frac{1}{4}\Delta t L(u^{(1)}), \quad (2.14b)$$

$$u^{n+1} = \frac{1}{3}u^n + \frac{2}{3}u^{(2)} + \frac{2}{3}\Delta t L(u^{(2)}). \quad (2.14c)$$

3. Accuracy, Stability and Conservative Error

In this section, we will present some theoretical analysis about the multi-domain hybrid DG and WENO-FD method described in Section 2. For the conservative coupling approach, analysis of accuracy and stability will be presented in Subsection 3.1. We also give a comparison between the two different choices, using the DG flux or using the WENO-FD flux, as the unique numerical flux at the coupling interface as shown in Fig. 3.1(a) and Fig. 3.1(b). For the non-conservative coupling approach, analysis of accuracy and conservative error will be presented in Subsection 3.2.

3.1. Conservative coupling approach

In the conservative coupling approach, an unique flux needs to be defined at the coupling interface. This can easily be done by simply choosing the numerical flux of either the DG method or the WENO-FD scheme provided at the interface. Another simple way is to use an

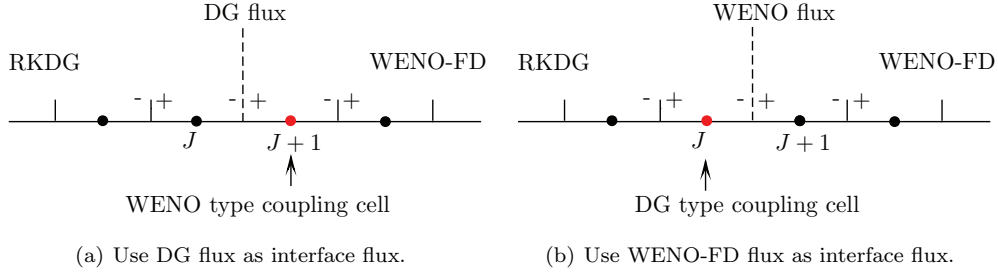


Fig. 3.1. Different choices of numerical flux at the coupling interface for conservative coupling.

exact or approximate Riemann problem solution to define a unique numerical flux since the left and right flow states at the coupling interface are readily provided by the DG and WENO methods. In this work, we simply take either the DG flux or the WENO-FD flux as the unique flux at coupling interface. If we apply the DG flux at the coupling interface $x = x_{J+1/2}$ as shown in Fig. 3.1(a), a so-called WENO type ‘coupling cell’ will be generated in the cell I_{J+1} which means the space discretization in the cell I_{J+1} is employed by WENO-FD schemes, however, the numerical flux of left boundary of this cell comes from DG method. In a similar way, if a WENO-FD flux is chosen as the unique flux at $x = x_{J+1/2}$, the ‘coupling cell’ will be located in the cell I_J with a DG discretization actually applied in it, we denote it as a DG type ‘coupling cell’ as shown in Fig. 3.1(b).

3.1.1. Accuracy analysis

We note that the space discretization in the coupling cell with these two different choices of numerical fluxes shown in Fig. 3.1(a) and Fig. 3.1(b), however, leads to a similar form. In specific, if the DG flux is employed at the coupling interface, the semi-discrete scheme for the WENO-FD point value u_{J+1} in the cell I_{J+1} follows

$$\frac{d}{dt}u_{J+1} + \frac{1}{\Delta x_{J+1}}(\tilde{f}_{J+\frac{3}{2}}^{(weno)} - \tilde{f}_{J+\frac{1}{2}}^{(rkdg)}) = 0. \quad (3.1)$$

Conversely, if the WENO-FD flux is used, the semi-discrete scheme for the DG cell average value u_J in the cell I_J has the form

$$\frac{d}{dt}u_J + \frac{1}{\Delta x_J}(\tilde{f}_{J+\frac{1}{2}}^{(weno)} - \tilde{f}_{J-\frac{1}{2}}^{(rkdg)}) = 0. \quad (3.2)$$

Eq. (3.1) and Eq. (3.2) indicate that the accuracy of conservative hybrid DG/WENO-FD method in the coupling cell is independent from the choices of different numerical fluxes at the coupling interface. For the accuracy analysis, we have the following theorem.

Theorem 3.1. *The semi-discrete scheme of the conservative coupling of a p^{th} -order ($p \geq 3$) DG method and a q^{th} -order ($q \geq 3$) WENO-FD scheme is of first order accuracy locally in the coupling cell in the norm L_∞ .*

Proof. To evaluate the numerical flux of a q^{th} -order WENO-FD scheme, we assign λ_k is the linear weight and p_k is the reconstructed polynomials of the candidate stencil S_k ($k = 0, 1, \dots, r-1$, $q = 2r-1$).

Then we have

$$\widehat{f}_{J+\frac{3}{2}}^{(weno)} = h_{J+\frac{3}{2}} + O(\Delta x^q), \quad (3.3)$$

where the definition of $h(x)$ is according to Shu and Osher [24, 25]:

$$f(x) = \frac{1}{\Delta x} \int_{x-\Delta x/2}^{x+\Delta x/2} h(\xi) d\xi. \quad (3.4)$$

For the p^{th} -order DG method, using Taylor series expansion at the center of the cell I_J reveals the following formula at the coupling interface

$$\widehat{f}_{J+\frac{1}{2}}^{(rkdg)} = f_{J+\frac{1}{2}} + O(\Delta x^p). \quad (3.5)$$

From Eq. (3.3) and Eq. (3.5), the space discretization in the cell I_{J+1} can be rewritten as

$$\widehat{f}_{J+\frac{3}{2}}^{(weno)} - \widehat{f}_{J+\frac{1}{2}}^{(rkdg)} = h_{J+\frac{3}{2}} - f_{J+\frac{1}{2}} + O(\Delta x^{\min(p,q)}). \quad (3.6)$$

From Shu and Osher [24, 25], we know that the relationship between $h_{J+\frac{3}{2}}$ and $f_{J+\frac{3}{2}}$ is

$$h_{J+\frac{3}{2}} = f_{J+\frac{3}{2}} - \frac{1}{24} \frac{d^2 f}{dx^2} \Big|_{x=x_{J+\frac{3}{2}}} \Delta x^2 + O(\Delta x^4). \quad (3.7)$$

Eq. (3.7) indicates that

$$\widehat{f}_{J+\frac{3}{2}}^{(weno)} - \widehat{f}_{J+\frac{1}{2}}^{(rkdg)} = f_{J+\frac{3}{2}} - f_{J+\frac{1}{2}} + O(\Delta x^2). \quad (3.8)$$

Thus, the semi-discrete scheme of the conservative hybrid approach in the coupling cell is of first order accuracy and the accuracy is independent from the choices of numerical fluxes used at the interface. \square

Remark 3.1. Although, the conservative semi-discrete scheme in the coupling cell is of first-order accuracy, an $O(\Delta x^2)$ solution error is routinely observed for the whole computation domain in numerical experiments after applying time discretization.

3.1.2. Stability

In this subsection, we present analysis of stability for the conservative coupling approach through numerical tests. The two different choices of numerical fluxes at the coupling interface do not exert much influence on the accuracy. Nevertheless, numerical experiments show that the stability of the conservative coupling approach in some degree depends on the choices of numerical fluxes.

In our numerical experiments, the linear scalar hyperbolic conservation law is used as examples and the computational domain is directly divided into two subdomains. We test both linear and nonlinear situation for the conservative coupling approach. Linear conservative coupling approach means that the nonlinear limiter of the DG method and nonlinear weights of the WENO-FD scheme are not taken into consideration. In contrast, the nonlinear conservative coupling approach indicates that the nonlinear factors may exert their influence in solving a linear conservation law.

From our numerical results, it has been found that the using of DG flux at the coupling interface for conservative coupling approach can preserve numerical stability well for both linear

and nonlinear situation. However, the choice of using WENO-FD flux at the coupling interface may lead to linear instability in some situation. In order to preserve numerical stability for this case, nonlinear factors in the DG method and the WENO-FD scheme must be taken into consideration. The details of the numerical results are shown in Table 3.1.

Table 3.1: Stability of conservative coupling approach.

	Left subdomain: DG		Right subdomain: WENO-FD	
	Use DG flux at coupling interface		Use WENO-FD flux at coupling interface	
	$f'(u) > 0$	$f'(u) < 0$	$f'(u) > 0$	$f'(u) < 0$
linear	✓	✓	×	✓
nonlinear	✓	✓	✓	✓
	Left subdomain: WENO-FD		Right subdomain: DG	
	Use DG flux at coupling interface		Use WENO-FD flux at coupling interface	
	$f'(u) > 0$	$f'(u) < 0$	$f'(u) > 0$	$f'(u) < 0$
linear	✓	✓	✓	×
nonlinear	✓	✓	✓	✓

3.2. Non-conservative coupling approach

For the non-conservative coupling approach, we give theoretical results of accuracy and local conservative error. The conclusion of accuracy analysis is directly given by the theorem ?? as the reconstruction steps are applied at the coupling interface, the fact that the non-conservative coupling approach can preserve high order accuracy for smooth solutions becomes obvious.

3.2.1. Accuracy analysis

The semi-discrete scheme of the non-conservative coupling of a p^{th} -order ($p \geq 3$) DG method and a q^{th} -order ($q \geq 3$) WENO-FD scheme can preserve optimal r^{th} -order ($r = \min\{p, q\}$) accuracy in the region of smooth solutions.

3.2.2. Conservative error

A significant concern of a non-conservative method is the conservative error (CE). Here, we use following formula to evaluate the local conservative error:

$$CE = \left| \sum_j \Delta x_j u_j^{n+1} - \sum_j \Delta x_j u_j^n \right|, \quad (3.9)$$

where u_j^n is the numerical solution of time T_n . If a one dimensional scheme is truly conservative with periodic boundary conditions or $\lim_{j \rightarrow \pm\infty} u_j^0 = 0$ is imposed, then the conservative error is equal to zero. For the non-conservative multi-domain hybrid DG/WENO-FD method, we give an analysis based on the definition above.

Theorem 3.2. *The local conservative error for the non-conservative coupling of a p^{th} -order ($p \geq 3$) DG method and a q^{th} -order ($q \geq 3$) WENO-FD scheme is of third order accuracy.*

Proof. From Eq. (2.11), we have

$$\begin{cases} u_j^{n+1} = u_j^n - \frac{\Delta t}{\Delta x} (\widehat{f}_{j+\frac{1}{2}}^{n(rkdg)} - \widehat{f}_{j-\frac{1}{2}}^{n(rkdg)}), & j = 1, \dots, J, \\ u_j^{n+1} = u_j^n - \frac{\Delta t}{\Delta x} (\widehat{f}_{j+\frac{1}{2}}^{n(weno)} - \widehat{f}_{j-\frac{1}{2}}^{n(weno)}), & j = J+1, \dots, N. \end{cases} \quad (3.10)$$

Multiply (3.10) by Δx and sum over all cells with the assumption that $j \rightarrow 1$ and $j \rightarrow N$, $u_j^0 \rightarrow 0$, we obtain

$$\sum_j \Delta x u_j^{n+1} - \sum_j \Delta x u_j^n = -\Delta t \left(\widehat{f}_{J+\frac{1}{2}}^{n(kdg)} - \widehat{f}_{J+\frac{1}{2}}^{n(weno)} \right). \quad (3.11)$$

As we known from theorem 3.1,

$$\left| \widehat{f}_{J+\frac{1}{2}}^{k(kdg)} - \widehat{f}_{J+\frac{1}{2}}^{k(weno)} \right| = O(\Delta x^2). \quad (3.12)$$

Thus, the conservative error of the non-conservative hybrid method is of third-order accuracy. \square

3.2.3. Stability

The strict theoretical analysis of stability for the non-conservative coupling approach may be complex and tedious. However, we can look at this problem from another point. As the DG method and WENO-FD scheme are both numerical stable, if we can preserve the property of essentially non-oscillatory in the reconstruction of numerical fluxes at the coupling interface, then the non-conservative coupling approach should preserve numerical stability. From the procedures of reconstructing numerical fluxes presented in Section 2.1, it should be noted that the WENO type reconstruction is applied to preserve the property of essentially non-oscillatory. Numerical experiments also demonstrate the non-conservative coupling approach is stable.

4. Numerical Results

In this section, we will present several numerical results of our high-order multi-domain hybrid DG/WENO-FD method. Two hybrid DG/WENO-FD methods are provided in Subsection 4.1 to verify the theoretical results for the conservative and non-conservative hybrid approaches, one is a hybrid 3^{rd} -order DG/ 5^{th} -order WENO-FD method, the other is a hybrid 5^{th} -order DG/ 5^{th} -order WENO-FD method. Then, typical cases of two dimensional scalar conservation law and Euler equations are presented to demonstrate the performance of our high-order hybrid solvers in Subsection 4.2 and 4.3.

4.1. One dimensional conservation law

4.1.1. Accuracy test

Example 4.1. We solve the linear advection equation with the following initial and exact boundary conditions:

$$\begin{cases} u_t - u_x = 0, \\ u(x, 0) = \sin(\pi(x + 0.25)). \end{cases} \quad x \in (0.0, 2.0), \quad (4.1)$$

In this test case, we display the accuracy results of the semi-discrete scheme for conservative coupling approach. In specific, a linear conservative coupling of third-order DG and fifth-order WENO-FD, together with a linear conservative coupling of fifth-order DG and fifth-order WENO-FD are demonstrated as examples. It should be noted that here compared to nonlinear coupling, linear coupling means the nonlinear factors, such as limiters in the DG subdomain and the nonlinear weights in the WENO-FD subdomain are not taken into account. The subdomain

Table 4.1: Accuracy test of the conservative coupling approach locally at the ‘coupling cell’ (Example 4.1).

N	Use DG flux at coupling interface				Use WENO-FD flux at coupling interface			
	3^{rd} -DG/ 5^{th} -WENO-FD	5^{th} -DG/ 5^{th} -WENO-FD	3^{rd} -DG/ 5^{th} -WENO-FD	5^{th} -DG/ 5^{th} -WENO-FD	3^{rd} -DG/ 5^{th} -WENO-FD	5^{th} -DG/ 5^{th} -WENO-FD	3^{rd} -DG/ 5^{th} -WENO-FD	5^{th} -DG/ 5^{th} -WENO-FD
	L_∞ error	L_∞ order	L_∞ error	L_∞ order	L_∞ error	L_∞ order	L_∞ error	L_∞ order
40	1.45E-2		1.45E-2		1.62E-2		1.66E-2	
80	7.27E-3	1.00	7.27E-3	1.00	7.71E-3	1.07	7.82E-3	1.09
160	3.63E-3	1.00	3.63E-3	1.00	3.75E-3	1.04	3.77E-3	1.05
320	1.82E-3	1.00	1.82E-3	1.00	1.85E-3	1.02	1.85E-3	1.03

interface is set at $x = 1.0$, where the DG method is applied in $(0.0, 1.0)$ and the WENO-FD scheme is applied in $(1.0, 2.0)$. At the coupling interface, we test both using the DG flux and using the WENO-FD flux as the unique flux for this conservative coupling approach. The results are shown in Table 4.1. Through the numerical results, we can see that the conservative semi-discrete coupling is locally first-order accuracy at the coupling cell and the order is independent from the choices of numerical fluxes at the coupling interface.

Example 4.2. We solve the linear advection equation with the following initial and exact boundary conditions:

$$\begin{cases} u_t - u_x = 0, \\ u(x, 0) = \sin(\pi(x + 0.25)). \end{cases} \quad x \in (0.0, 2.0), \quad (4.2)$$

In this test case, we display the results of a linear conservative coupling of third-order DG and the fifth-order WENO-FD, together with a linear conservative coupling of fifth-order DG and fifth-order WENO-FD. All the set are the same as Example 4.1. The computing time is till 1.0. At the coupling interface, we test both using the DG flux and using the WENO-FD flux as the unique flux for this conservative coupling approach. The results are shown in Table 4.2. Through the numerical results, we can see that the conservative coupling approach is numerical stable and shows upmost second-order accuracy in the whole computation domain and the order of accuracy is independent from the choices of numerical fluxes at the coupling interface.

Table 4.2: Accuracy test of linear conservative coupling approach (Example 4.2).

N	Use DG flux at coupling interface							
	3^{rd} -DG/ 5^{th} -WENO-FD				5^{th} -DG/ 5^{th} -WENO-FD			
	L_∞ error	L_∞ order	L_1 error	L_1 order	L_∞ error	L_∞ order	L_1 error	L_1 order
40	1.02E-3		6.43E-4		1.03E-3		6.51E-4	
80	2.56E-4	1.99	1.62E-4	1.99	2.57E-4	2.00	1.63E-4	2.00
160	6.42E-5	2.00	4.07E-5	1.99	6.42E-5	2.00	4.09E-5	1.99
320	1.61E-5	2.00	1.02E-5	2.00	1.61E-5	2.00	1.02E-5	2.00
N	Use WENO-FD flux at coupling interface							
	3^{rd} -DG/ 5^{th} -WENO-FD				5^{th} -DG/ 5^{th} -WENO-FD			
	L_∞ error	L_∞ order	L_1 error	L_1 order	L_∞ error	L_∞ order	L_1 error	L_1 order
40	1.05E-3		6.58E-4		1.06E-3		6.67E-4	
80	2.58E-4	2.02	1.64E-4	2.00	2.58E-4	2.04	1.65E-4	2.02
160	6.42E-5	2.01	4.10E-5	2.00	6.43E-5	2.00	4.11E-5	2.01
320	1.61E-5	2.00	1.02E-5	2.01	1.61E-5	2.00	1.02E-5	2.01

Example 4.3. We solve the linear advection equation with the following initial and exact boundary conditions:

$$\begin{cases} u_t + u_x = 0, \\ u(x, 0) = \sin(\pi(x + 0.25)). \end{cases} \quad x \in (0.0, 2.0), \quad (4.3)$$

In this test case, the characteristics propagate in an opposite direction compared to Example 4.1. We also display the results of a linear conservative coupling of third-order DG and fifth-order WENO-FD, together with a linear conservative coupling of fifth-order DG and fifth-order WENO-FD. All the other settings are the same as Example 4.1. The results are shown in Table 4.3. In this case, numerical results show that the linear conservative coupling approach which uses the DG flux at the coupling interface is stable and exhibit a second-order convergence. However, the conservative coupling approach which adopts the WENO-FD flux suffers numerical instability during the numerical experiment. In order to preserve the stability, nonlinear factors must be considered as shown in Subsection 4.1.3.

Table 4.3: Accuracy test of linear conservative coupling approach (Example 4.3).

N	Use DG flux at the coupling interface							
	3^{rd} -DG/ 5^{th} -WENO-FD				5^{th} -DG/ 5^{th} -WENO-FD			
	L_∞ error	L_∞ order	L_1 error	L_1 order	L_∞ error	L_∞ order	L_1 error	L_1 order
40	1.03E-3		6.44E-4		1.03E-3		6.42E-4	
80	2.57E-4	2.00	1.62E-4	1.99	2.57E-4	2.00	1.62E-4	1.99
160	6.43E-5	2.00	4.07E-5	1.99	6.42E-5	2.00	4.07E-5	1.99
320	1.61E-5	2.00	1.02E-5	2.00	1.61E-5	2.00	1.02E-5	2.00

Example 4.4. We solve the same linear advection equation using non-conservative coupling approach with the following initial and exact boundary conditions:

$$\begin{cases} u_t \pm u_x = 0, \\ u(x, 0) = \sin(\pi(x + 0.25)). \end{cases} \quad x \in (0.0, 2.0), \quad (4.4)$$

In this example, we test the accuracy of the non-conservative coupling approach. All the other settings are same as Example 4.1. The results are shown in Table 4.4. As we seen

Table 4.4: Accuracy test of linear non-conservative coupling approach (Example 4.4).

N	3^{rd} -DG/ 5^{th} -WENO-FD							
	$u_t + u_x = 0$				$u_t - u_x = 0$			
	L_∞ error	L_∞ order	L_1 error	L_1 order	L_∞ error	L_∞ order	L_1 error	L_1 order
40	1.91E-5		1.40E-5		2.01E-5		1.39E-5	
80	2.06E-5	3.21	1.80E-6	2.96	2.08E-6	3.27	1.76E-6	2.98
160	2.57E-5	3.00	2.27E-7	2.99	2.57E-7	3.02	2.24E-7	2.97
320	3.21E-5	3.00	2.83E-8	3.00	3.21E-8	3.00	2.82E-8	2.99
N	5^{th} -DG/ 5^{th} -WENO-FD							
	$u_t + u_x = 0$				$u_t - u_x = 0$			
	L_∞ error	L_∞ order	L_1 error	L_1 order	L_∞ error	L_∞ order	L_1 error	L_1 order
40	4.67E-6		1.40E-6		3.56E-6		1.33E-6	
80	1.53E-7	4.93	4.15E-8	5.08	1.29E-7	4.79	6.11E-8	4.44
160	4.92E-9	4.96	1.27E-9	5.03	4.01E-9	5.01	1.89E-9	5.01
320	1.58E-10	4.96	4.00E-11	4.95	1.25E-10	5.00	5.97E-11	4.98

from the numerical results, the non-conservative coupling approach are numerical stable and can preserve optimal order of accuracy. More specifically, a third-order convergence and a fifth-order convergence are exhibited by a non-conservative coupling of a third-order DG method with a fifth-order WENO-FD scheme and a non-conservative coupling of a fifth-order DG method with a fifth-order WENO-FD scheme, respectively.

Example 4.5. We solve the Burgers' equation with the following initial and periodic boundary conditions:

$$\begin{cases} u_t + (\frac{u^2}{2})_x = 0, \\ u(x, 0) = 0.5 + \sin(\pi x). \end{cases} \quad x \in (0.0, 2.0), \quad (4.5)$$

In this test case, we display the accuracy tests for both the conservative coupling approach and non-conservative coupling approach. The computational domain has been divided into three subdomains where the DG method is in (0.5, 1.5) and the WENO-FD scheme is applied in (0.0, 0.5) and (1.5, 2.0). Periodic boundary is imposed and the computing time is till $T = 0.5/\pi$ when the solution is still smooth. The results are shown in Table 4.5 and 4.6. Similarly, we observe that conservative coupling approach shows only second-order of accuracy and the accuracy is independent from the choices of numerical fluxes at the coupling interfaces. In contrast, the non-conservative coupling approach demonstrates a good performance in preserving high-order accuracy.

Table 4.5: Accuracy test of conservative coupling approach (Example 4.5).

Use DG flux at the coupling interface								
3^{rd} -DG/ 5^{th} -WENO-FD					5^{th} -DG/ 5^{th} -WENO-FD			
N	L_∞ error	L_∞ order	L_∞ error	L_∞ order	L_∞ error	L_∞ order	L_∞ error	L_∞ order
40	1.04E-3		2.79E-4		9.95E-4		1.13E-4	
80	2.79E-4	1.90	3.08E-5	2.13	2.86E-4	1.80	2.79E-5	2.02
160	6.99E-5	2.00	7.31E-6	2.07	7.50E-5	1.93	6.96E-6	2.01
320	1.78E-5	1.96	1.79E-6	2.03	1.81E-5	2.05	1.73E-5	2.01
Use WENO-FD flux at the coupling interface								
3^{rd} -DG/ 5^{th} -WENO-FD					5^{th} -DG/ 5^{th} -WENO-FD			
N	L_∞ error	L_∞ order	L_1 error	L_1 order	L_∞ error	L_∞ order	L_1 error	L_1 order
40	1.19E-3		1.72E-4		1.15E-3		1.58E-4	
80	3.34E-4	1.83	3.58E-5	2.27	3.32E-4	1.79	3.26E-4	2.27
160	8.48E-5	1.98	7.89E-6	2.18	8.61E-5	1.95	7.41E-5	2.14
320	2.10E-5	2.01	1.85E-6	2.01	1.81E-5	2.25	1.73E-5	2.10

Table 4.6: Accuracy test of non-conservative coupling approach (Example 4.5).

3^{rd} -DG/ 5^{th} -WENO-FD					5^{th} -DG/ 5^{th} -WENO-FD			
N	L_∞ error	L_∞ order	L_1 error	L_1 order	L_∞ error	L_∞ order	L_1 error	L_1 order
40	1.47E-4		1.73E-5		2.29E-6		3.15E-7	
80	2.56E-5	2.53	2.53E-6	2.77	7.66E-8	4.90	5.85E-9	5.75
160	3.61E-6	2.83	3.51E-7	2.85	8.45E-10	6.50	1.42E-10	5.36
320	4.80E-7	2.91	4.61E-8	2.93	2.55E-11	5.05	4.32E-12	5.05

4.1.2. Conservative error

Example 4.6. We solve the linear advection equation with the following initial and periodic boundary conditions:

$$\begin{cases} u_t \pm u_x = 0, \\ u(x, 0) = \sin(\pi(x + 0.25)). \end{cases} \quad x \in (0.0, 2.0), \quad (4.6)$$

In this test case, we display the local conservative error of a non-conservative coupling of third-order DG and fifth-order WENO-FD, together with a non-conservative coupling of fifth-order DG and fifth-order WENO-FD. In order to impose periodic boundary conditions, the computational domain has been divided into three subdomains as Example 4.5. The results are shown in Table 4.7. From the numerical results, we can find out that the local conservative error is third-order which verifies our theoretical analysis.

Table 4.7: Local conservative error test of non-conservative coupling approach (Example 4.6).

	3^{rd} -DG/ 5^{th} -WENO-FD				5^{th} -DG/ 5^{th} -WENO-FD			
	$u_t + u_x = 0$		$u_t - u_x = 0$		$u_t + u_x = 0$		$u_t - u_x = 0$	
N	L_∞ error	L_∞ order	L_∞ error	L_∞ order	L_∞ error	L_∞ order	L_∞ error	L_∞ order
40	8.40E-6		8.40E-6		2.31E-6		2.31E-6	
80	1.04E-6	3.01	1.03E-6	3.02	2.89E-7	3.00	2.89E-7	3.00
160	1.30E-7	3.00	1.30E-7	3.00	3.61E-8	3.00	3.61E-8	3.00
320	1.63E-8	3.00	1.63E-8	3.00	4.52E-9	3.00	4.52E-9	3.00

4.1.3. Stability

Example 4.7. We solve the linear advection equation with the following initial and exact boundary conditions:

$$\begin{cases} u_t + u_x = 0, \\ u(x, 0) = \sin(\pi(x + 0.25)). \end{cases} \quad x \in (0, 2), \quad (4.7)$$

This test case is the same as Example 4.3 in which the numerical results show that it is linear unstable if WENO-FD flux is employed as the unique flux for the conservative coupling approach. In order to preserve numerical stability, the conservative coupling approach has to be nonlinear even for solving linear conservation law. When the nonlinear factors are taken into consideration, the conservative coupling using WENO-FD flux at coupling interface can preserve numerical stability and the numerical results are shown in Table 4.8.

Table 4.8: Stability test of conservative coupling approach (Example 4.7).

	Use WENO-FD flux at the coupling interface							
	3^{rd} -DG/ 5^{th} -WENO-FD				5^{th} -DG/ 5^{th} -WENO-FD			
N	L_∞ error	L_∞ order	L_1 error	L_1 order	L_∞ error	L_∞ order	L_1 error	L_1 order
40	3.46e-3		8.27e-4		4.72e-3		2.47e-3	
80	1.31e-3	1.40	1.97e-4	2.06	1.20e-3	1.98	6.21e-4	1.99
160	4.07e-4	1.69	4.61e-5	2.09	3.05e-4	1.98	1.56e-5	1.99
320	8.22e-5	2.30	1.07e-5	2.11	7.69e-5	1.99	3.90e-6	2.00

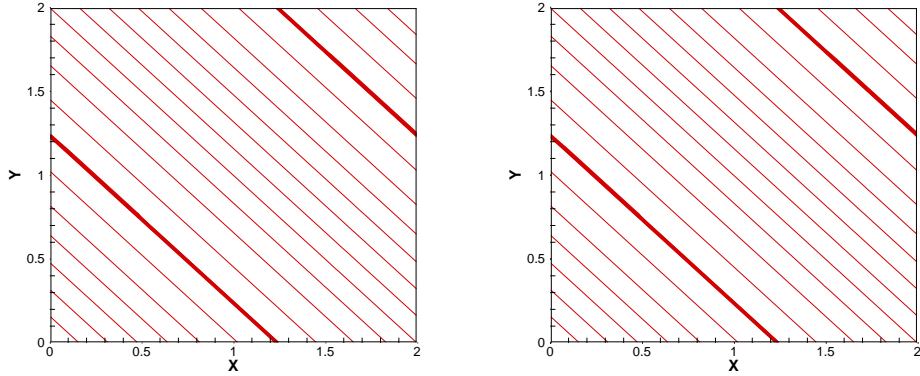
4.2. Two dimensional conservation law

Example 4.8. We further test the performance of the multi-domain hybrid DG/WENO-FD method for solving two dimensional inviscid Burgers' equation with the following initial and periodic boundary conditions. The subdomain interfaces occur at $x = 0.5, 0.0 < y < 2.0$ and $x = 1.5, 0.0 < y < 2.0$. The computing time is till $0.5/\pi$ and $1.5/\pi$. At $T = 0.5/\pi$, the solution is still smooth. We display the L_∞ and L_1 errors of a hybrid method of third-order DG coupling fifth-order WENO-FD together with a hybrid method of fifth-order DG coupling fifth-order WENO-FD, respectively. Numerical results show the hybrid methods can preserve high-order accuracy in Table 4.9. At $T = 1.5/\pi$, the numerical results illustrate that shock waves can correctly pass through the coupling interface as shown in Fig. 4.1.

$$\begin{cases} u_t + \left(\frac{u^2}{2}\right)_x + \left(\frac{u^2}{2}\right)_y = 0, \\ u(x, 0) = 0.5 \sin(\pi(x + y)) + 0.25. \end{cases} \quad (x, y) \in (0.0, 2.0) \times (0.0, 2.0), \quad (4.8)$$

Table 4.9: Accuracy test of hybrid DG/WENO-FD methods (Example 4.8).

N×N	3^{rd} -DG/ 5^{th} -WENO-FD				5^{th} -DG/ 5^{th} -WENO-FD			
	L_∞ error	L_∞ order	L_1 error	L_1 order	L_∞ error	L_∞ order	L_1 error	L_1 order
40×40	4.54e-4		2.96e-5		1.52e-4		2.95e-6	
80×80	5.10e-5	3.15	2.99e-6	3.31	9.60e-6	3.98	5.29e-8	5.80
160×160	3.44e-6	3.89	3.64e-7	3.11	3.93e-7	4.61	9.74e-10	5.76
320×320	4.90e-7	2.81	4.88e-8	2.90	1.03e-8	5.25	2.24e-11	5.44



(a) Hybrid 3^{rd} -DG/ 5^{th} -WENO-FD method, mesh size $h = 1/160$. (b) Hybrid 5^{th} -DG/ 5^{th} -WENO-FD method, mesh size $h = 1/160$.

Fig. 4.1. Two dimensional Burgers' equation at time $T = 1.5/\pi$.

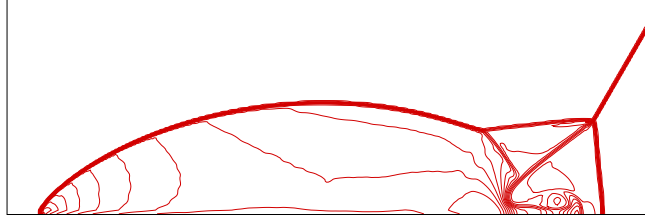
4.3. Two dimensional Euler equations

We consider the two dimensional Euler equations

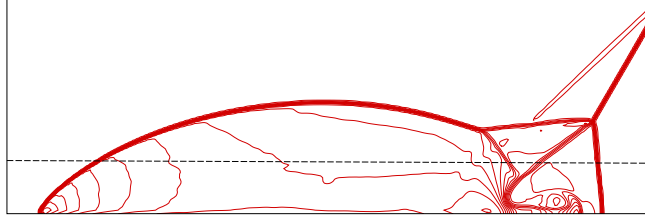
$$U_t + F(U)_x + G(U)_y = 0, \quad (4.9)$$

where

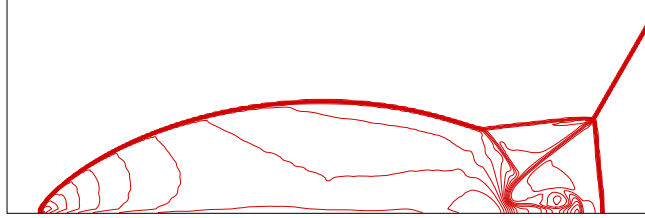
$$\begin{aligned} U &= (\rho, \rho u, \rho v, E)^T, \quad F(U) = (\rho u, \rho u^2 + P, \rho uv, u(E + P))^T, \\ G(U) &= (\rho v, \rho uv, \rho v^2 + P, v(E + P))^T. \end{aligned}$$



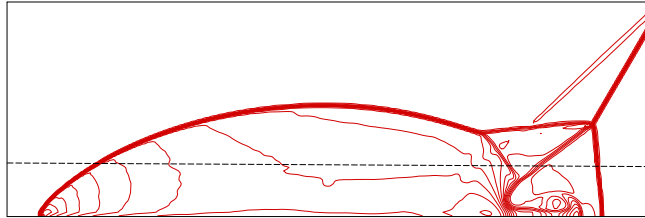
(a) 3^{rd} -DG method, 30 density contours from 1.731 to 20.92, mesh size $h = 1/120$, CPU time: 17059.6s



(b) Hybrid 3^{rd} -DG/ 5^{th} -WENO-FD method, 30 density contours from 1.731 to 20.92, mesh size $h = 1/120$, CPU time: 10238.7s



(c) 5^{th} -DG method, 30 density contours from 1.731 to 20.92, mesh size $h = 1/120$, CPU time: 75534.6s



(d) Hybrid 5^{th} -DG/ 5^{th} -WENO-FD method, 30 density contours from 1.731 to 20.92, mesh size $h = 1/120$, CPU time: 39921.2s

Fig. 4.2. Double mach reflection problem.

The total energy E is expressed as

$$E = \frac{P}{\gamma - 1} + \frac{1}{2}\rho(u^2 + v^2), \quad (4.10)$$

with $\gamma = 1.4$ for air.

Example 4.9. This is a standard test case for high resolution schemes. The computational domain is chosen to be $(0.0, 4.0) \times (0.0, 1.0)$. Initially a right-moving Mach 10 shock is positioned at $x = 1/6, y = 0.0$ and makes a 60° angle with the x -axis. The coupling interface is located at $y = 0.25, 0.0 < x < 4.0$ with DG method computing 25% regions of total domain near

the bottom. A comparison of the hybrid 3^{rd} -order DG/ 5^{th} -order WENO-FD method and the hybrid 5^{th} -order DG/ 5^{th} -order WENO-FD method is presented in Fig. 4.2. From the numerical results, we can see that both the third-order and the fifth-order hybrid DG/WENO-FD method give good performances in handling the coupling interface in this test case. From the CPU time comparison, it can be seen clearly that the hybrid method is much more efficient than traditional pure DG method.

5. Conclusions

In this paper, a general high-order multi-domain hybrid DG/WENO-FD method which couples a p^{th} -order ($p \geq 3$) DG method and a q^{th} -order ($q \geq 3$) WENO-FD scheme has been developed. The conservative and non-conservative coupling approaches were described in detail. We concluded that the conservative coupling approach is only of first-order accuracy locally at the ‘coupling cell’. In contrast, the non-conservative coupling approach can preserve the optimal order in the whole computation domain while the local conservative error is upmost third order. As for the stability analysis, numerical experiments showed nonlinear factors must be taken into consideration in order to maintain the stability for the conservative coupling approach when the WENO-FD flux is employed at the coupling interface. Further research focusing on extension the hybrid solver to diffusion equations is ongoing.

Acknowledgments. This work is supported by the Innovation Foundation of BUAA for PhD Graduates, the National Natural Science Foundation of China (Nos. 91130019 and 10931004), the International Cooperation Project (No. 2010DFR00700), the State Key Laboratory of Software Development Environment (No. SKLSDE-2011ZX-14) and the National 973 Project (No. 2012CB720205).

References

- [1] B. Cockburn, Discontinuous Galerkin methods for convection-dominated problems, High-order methods for computational physics, Springer Berlin Heidelberg, Springer, 1999.
- [2] B. Cockburn, C.-W. Shu, The Runge-Kutta local projection discontinuous Galerkin finite element method for scalar conservation laws V: Multidimensional systems, *J. Comput. Phys.*, **141**(1998), 199-224.
- [3] H. Luo, Y.D. Xia, S. Spiegel, R. Nourgaliev, Z. L. Jiang, A reconstructed discontinuous Galerkin method based on a Hierarchical WENO reconstruction for compressible flows on tetrahedral grids, *J. Comput. Phys.*, **236**(2013), 477-492.
- [4] J.X. Qiu, C.-W. Shu, Runge-Kutta discontinuous Galerkin method using WENO limiters, *SIAM J. Sci. Comput.*, **26**(2005), 907-929.
- [5] J.X. Qiu, C.-W. Shu, Hermite WENO schemes and their application as limiter for Runge-Kutta discontinuous Galerkin method: One dimensional case, *J. Comput. Phys.*, **193**(2004), 115-135.
- [6] J. Zhu, J.X. Qiu, Hermite WENO schemes and their application as limiter for Runge-Kutta discontinuous Galerkin method III: Unstructured meshes, *J. Sci. Comput.*, **39**(2009), 293-321.
- [7] H. Luo, J.D. Baum, R. Löhner, A Hermite WENO-based limiter for discontinuous Galerkin method on unstructured grids, *AIAA-2007-0510*.
- [8] H. Luo, Y. Xia, R. Nourgaliev, C. Cai, A Class of reconstructed discontinuous galerkin methods for the compressible flows on arbitrary grids, *AIAA-2011-0199*.
- [9] H. Luo, H. Xiao, R. Nourgaliev, C. Cai, A comparative study of different reconstruction schemes for reconstructed discontinuous Galerkin methods for the compressible flows on arbitrary grids, *AIAA-2011-3839*.
- [10] G.S. Jiang, C.-W. Shu, Efficient implementation of weighted ENO schemes, *J. Comput. Phys.*, **126**(1996), 202-228.

- [11] D. Balsara, C.-W. Shu, Monotonicity preserving weighted essentially non-oscillatory schemes with increasingly high order of accuracy, *J. Comput. Phys.*, **160**(2000), 405C452.
- [12] O. Friedrich, Weighted essentially non-oscillatory schemes for the interpolation of mean values on unstructured grids, *J. Comput. Phys.*, **144**(1998), 194-212.
- [13] Z.J. Wang, H.Y. Gao, A unifying lifting collocation penalty formulation including the discontinuous Galerkin, spectral volume/difference methods for conservation laws on mixed grids, *J. Comput. Phys.*, **228**(2009), 8161-8186.
- [14] Y. Liu, M. Vinokur, Z.J. Wang, Discontinuous spectral difference method for conservation laws on unstructured grids, *J. Comput. Phys.*, **216**(2006), 780-801.
- [15] M. Dumbser, D.S. Balsara, E.F. Toro, A unified framework for the construction of one step finite volume and discontinuous Galerkin schemes on unstructured meshes, *J. Comput. Phys.*, **227**(2008), 8209-8253.
- [16] L.P. Zhang, W. Liu, L.X. He, X.G. Deng, H.X. Zhang, A new class of DG/FV hybrid methods for conservation laws I: Basic formulation and one-dimensional systems, *J. Comput. Phys.*, **231**(2012), 1081-1103.
- [17] L.P. Zhang, W. Liu, L.X. He, X.G. Deng, H.X. Zhang, A class of hybrid DG/FV methods for conservation laws II: Two dimensional cases, *J. Comput. Phys.*, **231**(2012), 1104-1120.
- [18] L.P. Zhang, W. Liu, L.X. He, X.G. Deng, A class of hybrid DG/FV methods for conservation laws III: Two dimensional Euler Equations, *Commun. Comput. Phys.*, **12**(2012), 284-314.
- [19] Z.J. Wang, Spectral (Finite) volume method for conservation laws on unstructured grids: basic formulation, *J. Comput. Phys.*, **178**(2002), 210-251.
- [20] Z.J. Wang, Y. Liu, Spectral (Finite) volume method for conservation laws on unstructured grids IV: extension to two-dimensional systems, *J. Comput. Phys.*, **194**(2004), 716-741.
- [21] H.T. Huynh, A flux reconstruction approach to high-order schemes including discontinuous Galerkin methods, *AIAA-2007-4079*.
- [22] B. Costa, W.S. Don, Multi-domain hybrid spectral-WENO methods for hyperbolic conservation laws, *J. Comput. Phys.*, **224**(2007), 970-991.
- [23] K. Shahbazi, N. Albin, O.P. Bruno, J.S. Hesthaven, Multi-domain Fourier-continuation/WENO hybrid solver for conservation laws, *J. Comput. Phys.*, **230**(2011), 8779-8796.
- [24] C.-W. Shu, S. Osher, Efficient implementation of essentially non-oscillatory shock capturing schemes I, *J. Comput. Phys.*, **77**(1987), 439-471.
- [25] C.-W. Shu, S. Osher, Efficient implementation of essentially non-oscillatory shock capturing schemes II, *J. Comput. Phys.*, **83**(1989), 32-78.
- [26] J. Utzmann, F. Lörcher, M. Dumbser, C.-D. Munz, Aeroacoustic simulations for complex geometries based on hybrid meshes, *AIAA-2006-2418*.
- [27] R. Léger, C. Peyret, Coupled discontinuous Galerkin/Finite Difference solver on hybrid meshes for computational aeroacoustics, *AIAA JOURNAL* **50**(2012), 338-349.
- [28] J. Utzmann, T. Schwartzkopff, M. Dumbser, C.-D. Munz, Heterogeneous domain decomposition for CAA, *AIAA-2005-2989*.
- [29] P. Tsoutsanis, V.A. Titarev, D. Drikakis, WENO schemes on arbitrary mixed-element unstructured meshes in three space dimensions, *J. Comput. Phys.*, **230**(2011), 1585-1601.
- [30] M. Dumbser, M. Käser, Arbitrary high order non-oscillatory finite volume schemes on unstructured meshes for linear hyperbolic systems, *J. Comput. Phys.*, **221**(2007), 693-723.
- [31] J. Cheng, Y.W. Lu, T.G. Liu, Multi-domain hybrid RKDG and WENO methods for hyperbolic conservation laws, *SIAM J. Sci. Comput.*, **35**(2013), A1049-A1072.
- [32] J. Cheng, T.G. Liu, A multi-domain hybrid DG and WENO method for hyperbolic conservation laws on hybrid mesh, *Commun. Comput. Phys.*, **16**(2014), 1116-1134.
- [33] K. Sebastian and C.-W. Shu, Multidomain WENO finite difference method with interpolation at subdomain interfaces, *J. Sci. Comput.*, **19**(2003), 405-438.